

LA-UR- 11-06953

Approved for public release;  
distribution is unlimited.

*Title:* High-Speed Synchrotron X-Ray Phase Contrast Imaging for  
Analysis of Low-Z Composite Microstructure

*Author(s):* John D. Yeager  
Sheng-Nian Luo  
Brian J. Jensen  
Kamel Fezzaa  
David S. Montgomery  
Daniel E. Hooks

*Intended for:* Revised full length paper for Composites Part A: Applied  
Science and Manufacturing



Los Alamos National Laboratory, an affirmative action/equal opportunity employer, is operated by the Los Alamos National Security, LLC for the National Nuclear Security Administration of the U.S. Department of Energy under contract DE-AC52-06NA25396. By acceptance of this article, the publisher recognizes that the U.S. Government retains a nonexclusive, royalty-free license to publish or reproduce the published form of this contribution, or to allow others to do so, for U.S. Government purposes. Los Alamos National Laboratory requests that the publisher identify this article as work performed under the auspices of the U.S. Department of Energy. Los Alamos National Laboratory strongly supports academic freedom and a researcher's right to publish; as an institution, however, the Laboratory does not endorse the viewpoint of a publication or guarantee its technical correctness.

## High-Speed **Synchrotron** X-Ray Phase Contrast Imaging for Analysis of Low-Z Composite Microstructure

J. D. Yeager<sup>(a)\*</sup>, S. N. Luo<sup>(a)</sup>, B. J. Jensen<sup>(a)</sup>, K. Fezzaa<sup>(b)</sup>, D. S. Montgomery<sup>(a)</sup>, D. E. Hooks<sup>(a)</sup>

(a) Los Alamos National Laboratory, PO Box 1663, Los Alamos, NM 87545, USA

(b) X-Ray Science Division, Argonne National Laboratory, Argonne, IL 60439, USA

\* Corresponding Author: John D. Yeager, MS P952, PO Box 1663, Los Alamos, NM 87545, USA. Phone: +1 505 665 0879; Fax: +1 505 667 6372; Email: jyeager@lanl.gov.

### Abstract

The study of high performance composites such as plastic-bonded explosives under extreme conditions often requires innovative experimental techniques. Here, static **synchrotron x-ray** phase-contrast imaging (PCI) of simulated explosive materials has been performed at high speed in an effort to determine feasibility of imaging material response to dynamic, high-strain rate events ( $10^2 - 10^7 \text{ s}^{-1}$ ). The microstructure of pristine materials, idealized composites and simulated explosive composites has been characterized with synchrotron PCI at the Advanced Photon Source. High spatial resolution ( $2 \mu\text{m}$ ) of the microstructure was achieved with  $5 \mu\text{s}$  exposures, and features such as interfaces, cracks, voids, and bubbles were clearly observed. The likelihood of obtaining sufficient phase information at even faster exposures (e.g.  $0.2\text{-}0.5 \mu\text{s}$ ) is shown to be high.

Keywords: A. Polymer-matrix composites (PMCs); B. Interface/interphase; B. Microstructures; D. Radiography

## **1. Introduction**

Understanding and predicting detonation, failure and general deformation mechanisms in plastic-bonded explosive (PBX) composites is an important goal for the explosives community. PBX materials consist of micron-sized explosive crystals embedded in a polymer matrix. Typical formulation involves suspending the crystals in water and mixing the suspension with a polymer solution. The water crashes the dissolved polymer out of solution to create crystal-polymer agglomerate particles known as molding prills. The prills are then pressed to shape or compression molded into cylinders or pellets. The composites are highly loaded, usually greater than 85% crystals by weight, and both particle size and particle size distribution are known to affect the mechanical properties and detonation behavior [1-3]. The microstructure of PBX 9501, composed of 95% cyclotetramethylene-tetranitramine (HMX) crystals and 5% plasticized Estane 5703 by weight, is shown in Figure 1.

<Figure 1>

The microstructure of the PBX, and in particular the crystal-binder interface, plays an important role in mechanical deformation events, including failure. Defects within crystals, at the crystal-binder interface, in the partially dissolved crystal-binder region (“dirty binder”), or within the binder itself may all contribute to formation of local inhomogeneities (“hot spots”) which initiate deflagration or detonation [4, 5]. Crack propagation between the crystals and the binder has been observed in many systems and is usually the failure mechanism of PBX materials under mechanical strain [6-8]. PBXs are difficult to study at the micro-scale or nano-scale with conventional techniques due to the complexity of the microstructure, the brittle nature of the molecular crystals, the compositional (low-Z) similarities between the crystals and the binder,

and ease of thermal degradation or melting under an electron beam. The use of unique, innovative methods is often necessary to gather structural information for these materials.

X-ray study of composites is gaining in popularity as source and detector technology improves. Three dimensional (3D) applications such as tomography have been used recently to identify glass fiber orientation and distribution in sheet molding compounds [9] and reinforced polyamides [10] as well as microsphere and epoxy fracture in syntactic foams [11]. These tomography studies used phase contrast imaging (PCI) which allows greater contrast than traditional absorption radiography. For an excellent overview of the theoretical aspects of PCI, refer to the review by Wu and Liu [12]. While X-ray tube sources have been successfully used for PCI in structural materials [13], synchrotron sources provide orders of magnitude higher brightness and coherence [14], allowing for better contrast and sensitivity, and shorter exposure times for ultrafast dynamics studies [15]. Synchrotron PCI allows for quantitative measurement of the phase shift of a material without the need for interferometry [16]. With this technique, phase effects can be adjusted to optimize microstructural contrast and eliminate spurious features by simply changing the sample-to-detector distance, placing the sample behind a random phase screen, or by tilting the sample [17].

Experiments using PCI present exciting possibilities for observing high strain rate deformation (e.g., shock waves) at the microstructural scale in PBX materials. A previous study at the Advanced Photon Source (APS) at Argonne National Laboratory achieved 10  $\mu\text{m}$  spatial resolution of a tungsten – silicon reaction using ultrafast “white” radiation x-ray pulses and microsecond exposure times [18]. Our main objective in the current work was to assess the

feasibility of performing high-speed PCI measurements on low-Z materials to study microstructure and defects using the synchrotron X-ray beam at APS and available X-ray detectors. These initial measurements will guide future dynamic loading experiments which will use high-speed PCI to investigate microstructural effects on the dynamic response of PBXs or similar composites. In contrast to quasi-static loading, dynamic loading experiments can readily examine a material's response over a wide range of strain rates ( $10^2 \text{ s}^{-1}$  to  $10^7 \text{ s}^{-1}$ ) and timescales (ns to ms), making it possible to directly examine mechanical deformation in real time.

Although such dynamic experiments are of great interest to the high-pressure community, they pose significant technical challenges related to the use of x-ray detectors and x-ray sources mostly because of the short duration of the dynamic state, which significantly limits the number of photons available for detection. Synchronization of the dynamic event with the incoming photon bunches and the detector is also required. These difficulties coupled with the high costs of dynamic experiments warrant independent feasibility studies as presented here. Key targets of our study included determination of whether we could observe the microstructure at sufficient spatial and temporal resolution to study dynamic response and whether we needed to introduce a doping agent to achieve contrast between crystals and polymers. In addition, observation of cracks, voids, bubbles, or other defects would be particularly interesting. As a side benefit of our PCI feasibility study, we wanted to show that the technique could be useful for other types of low-Z composites, such as pharmaceutical tablets or polymer-matrix composites (PMCs).

## **2. Sample Preparation**

In order to demonstrate the usefulness of PCI to studying specific microstructural features, simulated PBX samples with engineered microstructures were fabricated with a variety of processes. Sucrose (J.T. Baker, Phillipsburg, NJ) and acetaminophen (Acros, Morris Plains, NJ) were grown as single crystals from water or ethanol solutions, following the method of Ramos et al. for the sucrose [19] and the method of Finnie et al. for the acetaminophen [20]. The acetaminophen tends to crystallize from solution by spiral growth, usually resulting in highly defective surfaces [21], while sucrose surfaces can generally be grown with smooth surfaces. Sucrose and acetaminophen were chosen as simulants for the explosive HMX because they have similar crystal structure (monoclinic), solubility in certain solvents, and mechanical properties. Some single crystals were embedded in Angstrom Bond epoxy (Fiber Optic Center, Inc., New Bedford, MA) or the poly(ester urethane) Estane 5703 (B.F. Goodrich, Jacksonville, FL), while others were bonded together with water or epoxy to study crystal-crystal interfaces. Estane was chosen because it used in some explosive formulations and has been well characterized previously [22]. Certain single crystals were intentionally damaged by creating a 250  $\mu\text{m}$  trench in one surface with a wire saw.

Sucrose powder was also formulated into a plastic-bonded simulant (PBS) pellet using an identical procedure to that for PBX 9501, including using an identical plasticized Estane binder at 5 wt% [6]. The effect of doping was studied by using  $\text{Bi}_2\text{O}_3$  nanoparticles (90-210 nm in diameter; MTI, Richmond, CA), **intended to enhance absorption** contrast in some polymer-embedded samples. **Doping is a common practice in x-ray tomography performed on biological samples; for example, gold is often used for enhanced absorption contrast due to attenuation of the beam during imaging of tumors or other tissue samples [23].** PBS pellets were produced

with a range of thicknesses and in some cases the PBS molding prills were doped prior to pressing. Additionally, binder cracking was simulated by intentionally cracking a polymethylmethacrylate (PMMA) slab. General sample size along the probing direction was between 0.3 and 3.5 mm. A list of all studied samples is given in Table 1.

<Table 1>

### **3. X-ray Characterization Experiments**

PCI is much more effective for imaging than traditional radiography especially for low-Z materials. The complex index of refraction of a material for x-rays is  $n=1-\delta-i\beta$  where  $\beta$  accounts for absorption, and  $\delta$  contains phase information [12]. Traditional x-ray radiography relies on the spatial variation of  $\beta$  to produce the intensity variation in the image, while PCI relies on the  $\delta$  variation. More precisely, the second derivative (or Laplacian) of the phase modulates the intensity after a finite propagation distance, and can be used for imaging the object microstructure. **The weak absorption contrast of low-Z materials is enhanced by measurement of phase effects with PCI, and is particularly useful for structural materials such as glass fibers or polymers [24].** PCI requires a (partial) degree of spatial coherence for the x-ray beam, but depends weakly on spectral coherence, so there is no requirement for a monochromatic source. Thus, the use of synchrotron radiation without a monochromator is possible for high-speed PCI.

Prior to PCI measurements at the APS, several of the samples were characterized by radiography-based tomography at Los Alamos National Laboratory. Specimens PBS-1 and ENG-3 were **examined** with an in-house tungsten anode x-ray source operated at 150 kV. **Series of 2D absorption radiographs were obtained while rotating the sample, and then the angular projections were used to reconstruct a 3D image.**

PCI experiments were performed under ambient conditions at 32ID-B beamline of the APS. The experimental configuration is shown in Figure 2. The PCI method used a “white” beam which was transmitted through the composite material or single crystal samples and then imaged onto a camera. The storage ring was operating in the standard mode (24 bunches), with pulses of 40 ps duration spaced 153 ns apart [25]. The beam intensity and spectra were adjustable by varying the undulator gap with typical operation in the 11-30 mm range. Most of our measurements used an undulator gap of 20 mm. For this gap, the majority of the intensity was located in the first harmonic centered around 9 keV with a bandwidth of 0.4 keV FWHM, and the peak radiance was about  $3 \times 10^{14}$  photons/s/0.1%bw (see Figure 2b). **More detailed specifications of the beamline design are found in Shen et al [26].** Two electromechanical shutters (slow and fast) and a slit were placed between the x-ray source and the sample, conditioning the beam temporally and spatially for imaging and controlling the area of illumination on the sample. The slow shutter absorbs more than 99% of the power (to protect samples and diagnostics downstream from beam damage) and the beam goes through for a few milliseconds at a rate of 1 Hz. During this wide time window, the fast shutter produces a narrow time window of **100  $\mu$ s** for imaging, **while the actual exposure time was set by the fast CCD camera to about 5  $\mu$ s**. Both shutters were timed against a time-zero reference supplied by the synchrotron storage ring (RF signal), with appropriate delays controlled by a Stanford Research Systems (SRS) DG535 delay boxes. The illumination area on the sample was controlled with the slit(s). **A LuAG:Ce** scintillator was positioned downstream 120 mm away from the sample. A 45° mirror relayed the optical emission from the scintillator into the recording SensiCam camera (Cooke; 6.3  $\mu$ m $\times$ 6.3  $\mu$ m pixel size, and 1280 $\times$ 1024 pixels), through a 10 $\times$  microscope objective. The field of view on

the sample was approximately 0.85 mm×0.65 mm. The beam was aligned with a foam target and spatial calibration was achieved by use of a 63.5 μm period gold grid. Resolution for the PCI setup (including the detector point spread function and the geometrical blurring from the source size) was determined to be approximately 2-4 μm. The background intensity was about 80 counts (noise level).

<Figure 2>

## **4. Results**

### **4.1 Single Material Characterization**

Samples consisting of single crystals or single polymers were characterized in terms of the ability to resolve microstructure and signal to noise ratio (S/N). The strength of the signal is described here by the number of counts the detector records. PCI results are shown in Figure 3 for sucrose and acetaminophen single crystals and in Figure 4 for PMMA and Estane (in PBS-1 sample), and S/N is about 25.

<Figure 3>

In Figure 3, the edges of the crystals are clearly defined and heterogeneities within the crystal are visible as well. For PMMA and Estane (Figure 4), suitable intensity was obtained throughout both specimens, and the images displayed in the figure were chosen to emphasize the ability to observe defects in high resolution. The images are from within the bulk of the polymers, showing internal crack branching and voids. Recall that PCI is a projection technique, so overlapping features are actually at different depths in the sample.

<Figure 4>

#### 4.2 Engineered Sample Characterization

The feasibility of studying interfacial phenomena in detail was assessed with the acetaminophen crystal-crystal samples (or “bicrystals”), ENG-1 and ENG-2. Figure 5 focuses on the bicrystal interface in the ENG-1 sample, showing sufficient contrast to resolve the boundaries of each crystal along with various bulk and surface imperfections such as curvature and growth spirals. Both crystals in ENG-1 show high roughness at the surface and noticeable bulk defects. The dark band at the surface of Crystal 2 was probably a result of slight tilting of the sample with respect to the beam axis.

<Figure 5>

The epoxy-bonded bicrystal ENG-2 was characterized with similar resolution to ENG-1 but provided additional insight into polymer-crystal delamination events (Figure 6). The large acetaminophen crystals had curved surfaces, and when the surfaces were joined by epoxy they appeared to relax over the duration of the cure time. This resulted in epoxy delamination from the crystal, simulating commonly observed crystal-binder delamination in PBX materials under small tensile loads [2].

<Figure 6>

Fig. 6 appears to show delamination of the epoxy from both crystals. Certainly Crystal 1 has pulled away from the epoxy during the curing stage, but it appears to have initially pulled the epoxy off of Crystal 2 to form a buckle. Another possibility for the buckle formation is that

Crystal 2 may have been moved sideways during the cure and caused a pileup of epoxy at the edge of the crystal. Either way, polymer-crystal delamination is well resolved with PCI.

ENG-1 and ENG-2 characterization proved the feasibility of imaging interfaces and small surface defects. However, crystal-crystal regions in typical PBX formulations are rarely as smooth as these engineered samples. ENG-3, the bicrystal with a machined trench, was a step towards real crystal surface imperfections. In order to understand the projection view obtainable with PCI, we first characterized the sample with radiographic microtomography using a laboratory source. Preliminary results revealed that acetaminophen crystals were almost indistinguishable from the epoxy. For ENG-3,  $\text{Bi}_2\text{O}_3$  nanoparticles were added to highlight the crystal-epoxy interface by differential beam attenuation. Unfortunately, the doping was only partially successful because some nanoparticles tended to agglomerate when mixed in the epoxy. The high attenuation and hardening of x-ray beam caused by the large agglomerates generated numerous artifacts in the reconstructed 3D images. However, we were able to find regions of interest in the sample on the longitudinal center of the trench, with little to no large agglomerates. We used standard local-tomography algorithms to reconstruct higher quality images. Figure 7 compares a tomography slice with PCI, showing the bicrystal interface and the trench in a side-on view. The tomography provided limited contrast related to the composite structure and  $\text{Bi}_2\text{O}_3$  particle distribution, while we were able to well discern  $\text{Bi}_2\text{O}_3$  distribution in the epoxy-filled trench with PCI, as well as surrounding the crystals (not shown).

<Figure 7>

It should be noted that the lateral spatial resolution is higher for PCI (~2  $\mu\text{m}$ ) than for tomography. The **image quality is a function of detection resolution and contrast mechanism**, both of which are superior in synchrotron PCI. In principle, PCI tomography can be done in such a way as to achieve **2  $\mu\text{m}$  resolution with sub-second acquisition time per set** [27]. Alternatively, flash radiography can provide similar resolution at millisecond exposure times [28]. However, no technique currently exists that can provide full 3D phase information with micron spatial resolution and nano-to-microsecond temporal resolution. Within the limitations of current technology, synchrotron PCI appears to be the best option for high-speed study of these low-Z composites.

#### *4.3 Plastic-Bonded Simulant Composites*

We were able to observe crystals, polymer, voids, and cracks in the pressed Estane pellet, PBS-1. Half of the embedded crystals had been doped with  $\text{Bi}_2\text{O}_3$  to assess the necessity of using dopant to achieve contrast. This sample had been previously characterized by x-ray tomography at LANL, and the transparency of the Estane allowed for some optical observation as well. Figure 8 is a comparison between x-ray tomography, optical microscopy and PCI.

<Figure 8>

The dopant appears to be necessary to achieve contrast with the x-ray absorption tomography while it only mildly assists interfacial resolution in the PCI. Despite imaging through the thickness of the sample, PCI reveals fracture within the crystals and extensive void formation around the crystals. Both of these defect structures are likely caused by the high flow stress

necessary to shape the original Estane particles into a pellet. PBS-1 was manufactured by pressing millimeter sized Estane particles around several acetaminophen crystals, rather than the wet agglomeration process described earlier, and this change in formulation conditions probably resulted in unusual stress conditions at the crystal-polymer interface. While the processing did not precisely replicate PBX formulation, the observations possible with PCI are both indicative of expected features and likely to be of equivalent utility in future measurements in actual formulations. Further, the excellent **contrast due to the microstructure** implies that with proper experimental approach, sample geometry, and fast detector advancements, the photon flux is sufficient to perform dynamic observations of failure events.

PBS-2 and PBS-3 were made with identical formulation parameters to PBX 9501 but were somewhat difficult to image. The results of both samples, doped and non-doped, are shown in Figure 9. It is instructive to compare the microstructure from Figure 9 to the PBX microstructure from Figure 1 in order to understand the imaging concerns.

<Figure 9>

Noting that both the PBS samples were approximately 2 millimeters thick, we addressed the problem by slicing off thin pieces with a razor. Figure 10 shows the same samples as Figure 9 after slicing to a thickness of approximately 400  $\mu\text{m}$ .

<Figure 10>

**Samples in Figure 9a behave like a weakly absorbing (phase) object, with a very large number of small crystals in the x-ray beam path. The dominant length-scale estimated from the images to be**

on the order of 10  $\mu\text{m}$ . Given the values of the imaging distance (defocus  $\sim 0.12$  m) and the x-ray wavelength (0.14 nm), the order of magnitude of the Fresnel number is  $\sim 1$ . Since the synchrotron x-ray beam is partially coherent, the contrast (sharp variations) can be attributed to speckle formation via coherent scattering in the forward direction. There is certainly an incoherent component, but its contribution is a very slowly varying background. The image formation in this regime can readily be simulated using the Fresnel approximation as indicated in, e.g., Kitchen et al [29]. The larger crystals (many tens of microns) have a uniform contribution to the image except for their edges, so they would not be distinguishable in a “random” speckle background (Figure 9a) but start to become visible when the sample thickness is reduced as in Figure 10a. As for Figure 9b, the weakly absorbing assumption is not valid anymore due to the dopant, and the sample does not behave as a “pure” phase object. Instead of a sharp speckle pattern, we observe mostly a smoother absorption contrast of the heavy nanoparticles. The distinction between different components in the doped sample is also enhanced with a reduced thickness (Figure 10b).

The thinner samples provided much better absolute intensity ( $\sim 1500$  counts). Most of the contrast in the non-doped composite (Figure 10a) arises from the small crystal interfaces but several large crystals are mostly visible. The doped composite reveals a different microstructure previously unobservable. The dopant appeared to surround the molding prills, the crystal-polymer agglomerates, rather than migrate to the crystal-polymer interface. This conclusion was reached by comparing the observed microstructure to the faceted crystal morphology from Figure 1. The dopant also showed a tendency to clump; note that the  $\text{Bi}_2\text{O}_3$  was a nanopowder before mixing with the PBS molding prills but regions of high concentrations in Figure 10b are

hundreds of microns across. This indicates that the presence of the powder may have affected the pressing behavior of the PBS agglomerates, or that the pressing process induces much less polymer flow around crystals than has been previously suspected. Contrasting doped vs. non-doped samples may be of use to study the effect of changing processing parameters on resulting composite microstructure.

### **5. Implications for dynamic experiments**

We found that single materials and engineered composite samples could be studied in great detail with the current x-ray detector setup at APS. High **quality images were obtained even** at very fast (5  $\mu$ s) exposure times. We clearly observed defects such as internal cracks, voids, air bubbles, surface imperfections, and polymer delamination.

Our high-speed PCI measurements at ambient conditions show promises as well as limitations in resolving *in situ* microstructure in dynamic experiments at APS-type synchrotrons. The key parameter is S/N, determined by the exposure time as required by specific dynamic experiments, beam characteristics (mostly synchrotron operation mode), sample type, and probing thickness, as well as scintillators and x-ray **or optical** cameras. For the current detector system, a minimum S/N of 3 corresponds to  $I_{\min}=240$  counts. We easily exceeded this minimum with 5  $\mu$ s exposure times for our simulated PBX samples. However, the feasibility of keeping an adequate S/N when trimming the exposure time to capture shock events ( $\sim 0.5$   $\mu$ s **or less**) needs to be discussed.

We take the nominal intensity in current setup as  $I_0=2500$  counts for 5  $\mu$ s exposure time in the standard mode (102 mA in 24 bunches during 3.68  $\mu$ s; the bunch separation is 153 ns). It

requires about 3 bunches in the standard mode to obtain  $I_{\min}$ ; 3 bunches in the standard mode correspond to a camera gate width of 307 ns. Thus, for the current detector and the standard mode, the “exposure time” (image integrated over this period from multiple bunches) will be at least 0.3  $\mu\text{s}$ . The standard mode operation should be sufficient for study of a wide range of dynamic experiments, but APS also offers an alternative operation mode. The hybrid or singlet mode at APS has different time structure of the probing beam. In the hybrid mode, a singlet pulse (16 mA, 65 ps pulse duration) is separated from septuplet pulses (86 mA and 470 ns in total) by 1.594  $\mu\text{s}$  on either side. The singlet is more desirable for time resolution due to the 65 ps duration, but synchronizing a highly dynamic event (0.2-0.5  $\mu\text{s}$  duration) with this pulse is likely to be very difficult. Additionally, achieving sufficient S/N requires capturing information from more than one singlet, which will require several  $\mu\text{s}$  event duration. The singlet mode is likely to be most useful for dynamic experiments at medium to low strain rates ( $10^2 - 10^4 \text{ s}^{-1}$ ). Improving the detector sensitivity or increasing photon fluxes may reduce the exposure time for both standard and hybrid modes at APS to allow for higher strain rate experiments.

One potential concern for dynamic experiments was the difficulty of imaging the simulated PBX composites at thicknesses greater than 1 mm. Sufficient contrast for revealing the microstructure was not reached even with 400  $\mu\text{m}$  thick samples. Adequate sample dimensions are necessary to achieve a sufficiently long, stable state (e.g., supported shock duration) and thus the required exposure time for PCI. However, sample dimensions and exposure times for dynamic study will be tailored to specific loading scenarios, such as drop weight, split Hopkinson pressure bar or Kolsky bar, or gas gun experiments [30-32]. For non-shock strain rate experiments, meaning slower dynamic loading, the exposure time can be correspondingly longer. It is possible that

complex microstructures could still be studied with PCI under such conditions. For our purposes, initial efforts on dynamic PCI should be focused on simple microstructures or engineered interfaces with elemental deformation processes.

## **6. Conclusions**

PCI has proven to be quite useful for imaging non-transparent simulated plastic-bonded explosives. PCI is superior to absorption radiography in terms of contrast and doping requirements. Doping is not necessary to achieve contrast between similar materials or within composites but can show a different structure (i.e. structure of molding prills rather than crystals). We demonstrate that sufficient contrast and intensity can be achieved for low-Z composites with the APS X-ray source in the standard operation mode and that dynamic study at high strain rates is feasible. Synchrotron PCI should be able to reveal the response of preexisting microstructure to shock loading. Specifically, void nucleation and collapse, fracture delamination, grain boundary/interface deformation, and hot spot formation may be studied with high temporal and spatial resolution. In addition, PCI may be useful for imaging mechanical or chemical behavior of other low-Z composites, statically or dynamically, even at microsecond time scales.

## **Acknowledgements**

The authors would like to thank B. Patterson (LANL) for help with x-ray tomography and sample discussions. Use of the Advanced Photon Source, an Office of Science User Facility operated for the U.S. Department of Energy (DOE) Office of Science by Argonne National Laboratory, was supported by the U.S. DOE under Contract No. DE-AC02-06CH11357. This

work was performed, in part, at the Center for Integrated Nanotechnologies, a U.S. Department of Energy, Office of Basic Energy Sciences user facility. **We are grateful for the support from Science Campaign and LDRD programs at Los Alamos National Laboratory.** Los Alamos National Laboratory, an affirmative action equal opportunity employer, is operated by Los Alamos National Security, LLC, for the National Nuclear Security Administration of the U.S. Department of Energy under contract DE-AC52-06NA25396.

#### References

- [1] Khasainov BA, Ermolaev BS, Presles HN, Vidal P. On the effect of grain size on shock sensitivity of heterogeneous high explosives. *Shock Waves*. 1997;7(2):89-105.
- [2] Palmer SJP, Field JE, Huntley JM. Deformation, Strengths and Strains to Failure of Polymer Bonded Explosives. *Proc R Soc London, Ser A*. 1993;440(1909):399-419.
- [3] Rae PJ, Palmer SJP, Goldrein HT, Field JE, Lewis AL. Quasi-static studies of the deformation and failure of PBX 9501. *Proc R Soc London, Ser A*. 2002;458(2025):2227-42.
- [4] Field JE, Bourne NK, Palmer SJP, Walley SM, Sharma J, Beard BC. Hot-Spot Ignition Mechanisms for Explosives and Propellants [and Discussion]. *Philosophical Transactions: Physical Sciences and Engineering*. 1992;339(1654):269-83.
- [5] Berghout HL, Son SF, Skidmore CB, Idar DJ, Asay BW. Combustion of damaged PBX 9501 explosive. *Thermochim Acta*. 2002;384(1-2):261-77.
- [6] Rae PJ, Goldrein HT, Palmer SJP, Field JE, Lewis AL. Quasi-Static Studies of the Deformation and Failure of b-HMX Based Polymer Bonded Explosives. *Proceedings: Mathematical, Physical and Engineering Sciences*. 2002;458(2019):743-62.
- [7] Chen P, Xie H, Huang F, Huang T, Ding Y. Deformation and failure of polymer bonded explosives under diametric compression test. *Polym Test*. 2006;25(3):333-41.
- [8] Liu ZW, Xie HM, Li KX, Chen PW, Huang FL. Fracture behavior of PBX simulation subject to combined thermal and mechanical loads. *Polym Test*. 2009;28(6):627-35.
- [9] Le TH, Dumont PJJ, Orgéas L, Favier D, Salvo L, Boller E. X-ray phase contrast microtomography for the analysis of the fibrous microstructure of SMC composites. *Composites Part A: Applied Science and Manufacturing*. 2008;39(1):91-103.
- [10] Bernasconi A, Cosmi F, Dreossi D. Local anisotropy analysis of injection moulded fibre reinforced polymer composites. *Compos Sci Technol*. 2008;68(12):2574-81.
- [11] Awaja F, Arhatari BD. X-ray Micro Computed Tomography investigation of accelerated thermal degradation of epoxy resin/glass microsphere syntactic foam. *Composites Part A: Applied Science and Manufacturing*. 2009;40(8):1217-22.

- [12] Wu X, Liu H. Clinical implementation of x-ray phase-contrast imaging: Theoretical foundations and design considerations. *Medical Physics*. 2003;30(8):2169-79.
- [13] Zoofan B, Kim JY, Rokhlin SI, Frankel GS. Phase-contrast x-ray imaging for nondestructive evaluation of materials. *J Appl Phys*. 2006;100(1):014502-7.
- [14] Snigirev A, Snigireva I, Kohn V, Kuznetsov S, Schelokov I. On the possibilities of x-ray phase contrast microimaging by coherent high-energy synchrotron radiation. *Rev Sci Instrum*. 1995;66(12):5486-92.
- [15] Wang Y, Liu X, Im K-S, Lee W-K, Wang J, Fezzaa K, et al. Ultrafast X-ray study of dense-liquid-jet flow dynamics using structure-tracking velocimetry. *Nat Phys*. 2008;4(4):305-9.
- [16] Nugent KA, Gureyev TE, Cookson DF, Paganin D, Barnea Z. Quantitative Phase Imaging Using Hard X Rays. *Phys Rev Lett*. 1996;77(14):2961-4.
- [17] Cloetens P, Barrett R, Baruchel J, Guigay J-P, Schlenker M. Phase objects in synchrotron radiation hard x-ray imaging. *J Phys D: Appl Phys*. 1996;29(1):133.
- [18] Reeves RV, White JDE, Dufresne EM, Fezzaa K, Son SF, Varma A, et al. Microstructural transformations and kinetics of high-temperature heterogeneous gasless reactions by high-speed x-ray phase-contrast imaging. *Physical Review B*. 2009;80(22):224103.
- [19] Ramos KJ, Bahr DF. Mechanical behavior assessment of sucrose using nanoindentation. *J Mater Res*. 2007;22(7):9.
- [20] Finnie S, Prasad K, Sheen D, Sherwood J. Microhardness and Dislocation Identification Studies on Paracetamol Single Crystals. *Pharm Res*. 2001;18(5):674-81.
- [21] Ristic RI, Finnie S, Sheen DB, Sherwood JN. Macro- and Micromorphology of Monoclinic Paracetamol Grown from Pure Aqueous Solution. *The Journal of Physical Chemistry B*. 2001;105(38):9057-66.
- [22] Mang JT, Hjelm RP, Orler EB, Wroblewski DA. Small-Angle Neutron Scattering of a Solvent-Swollen Segmented Polyurethane as a Probe of Solvent Distribution and Polymer Domain Composition. *Macromolecules*. 2008;41(12):4358-70.
- [23] Popovtzer R, Agrawal A, Kotov NA, Popovtzer A, Balter J, Carey TE, et al. Targeted Gold Nanoparticles Enable Molecular CT Imaging of Cancer. *Nano Lett*. 2008;8(12):4593-6.
- [24] Wilkins SW, Gureyev TE, Gao D, Pogany A, Stevenson AW. Phase-contrast imaging using polychromatic hard X-rays. *Nature*. 1996;384(6607):335-8.
- [25] Sajaev VV. Storage Ring Operation Modes. [http://aps.anl.gov/Facility/Storage\\_Ring\\_Parameters/node5.html](http://aps.anl.gov/Facility/Storage_Ring_Parameters/node5.html). Accessed 05/09/2011 2011.
- [26] Shen Q, Lee W-K, Fezzaa K, Chu YS, De Carlo F, Jemian P, et al. Dedicated full-field X-ray imaging beamline at Advanced Photon Source. *Nuclear Instruments and Methods in Physics Research Section A: Accelerators, Spectrometers, Detectors and Associated Equipment*. 2007;582(1):77-9.
- [27] Baruchel J, Buffiere J-Y, Cloetens P, Di Michiel M, Ferrie E, Ludwig W, et al. Advances in synchrotron radiation microtomography. *Scripta Mater*. 2006;55(1):41-6.
- [28] Zhou S-A, Brahme A. Development of phase-contrast X-ray imaging techniques and potential medical applications. *Physica Medica*. 2008;24(3):129-48.
- [29] Kitchen MJ, Paganin D, Lewis RA, Yagi N, Uesugi K, Mudie ST. On the origin of speckle in x-ray phase contrast images of lung tissue. *Physics in Medicine and Biology*. 2004;49(18):4335.
- [30] Meyers MA. *Dynamic behavior of materials*. Wiley; 1994. p. 271-95.
- [31] Goldsmith W. *Impact: the theory and physical behaviour of colliding solids*. Dover Publications; 2001. p. 145-242.

[32] Kolsky H. An Investigation of the Mechanical Properties of Materials at very High Rates of Loading. Proceedings of the Physical Society Section B. 1949;62(11):676.

## Figures and Figure Captions

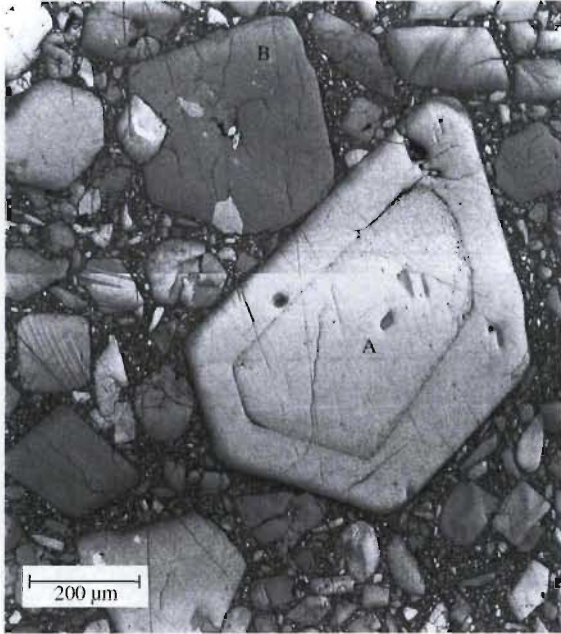


Figure 1. Microstructure of PBX 9501, showing a wide distribution of particle sizes and variability in crystal integrity: “A” is relatively defect free, while “B” contains inclusions. From Rae et al., used with permission [3].

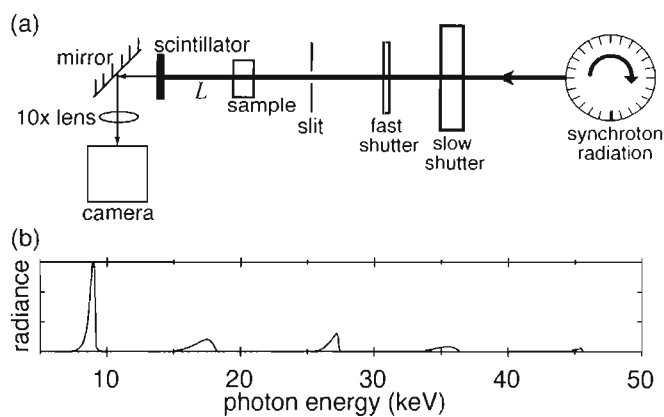


Figure 2. (a) Schematic of the experimental setup for PCI at APS 32ID-B. The synchrotron storage ring was operated in the standard mode. The sample-scintillator distance ( $L$ ) was 120

mm. (b) A simulated photon spectrum at 32ID-B for an undulator gap of 20 mm. Each division on the vertical axis represents  $10^{14}$  photons/s/0.1% bandwidth.

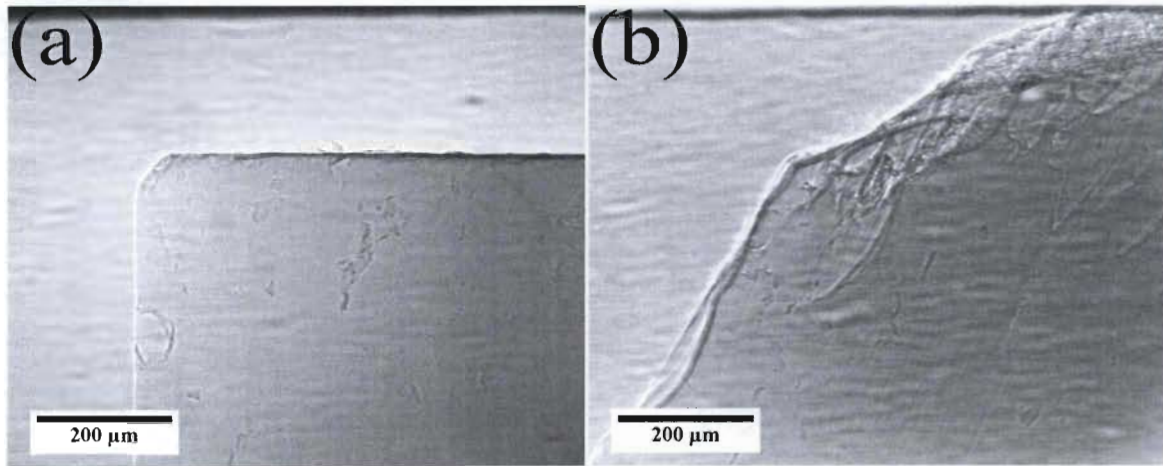


Figure 3. PCI at the crystal edge for sucrose (a) and acetaminophen (b), showing clearly observable morphology, surface imperfections, and bulk defects. The intensity is about 2400 counts (a) and 2000 counts (b).

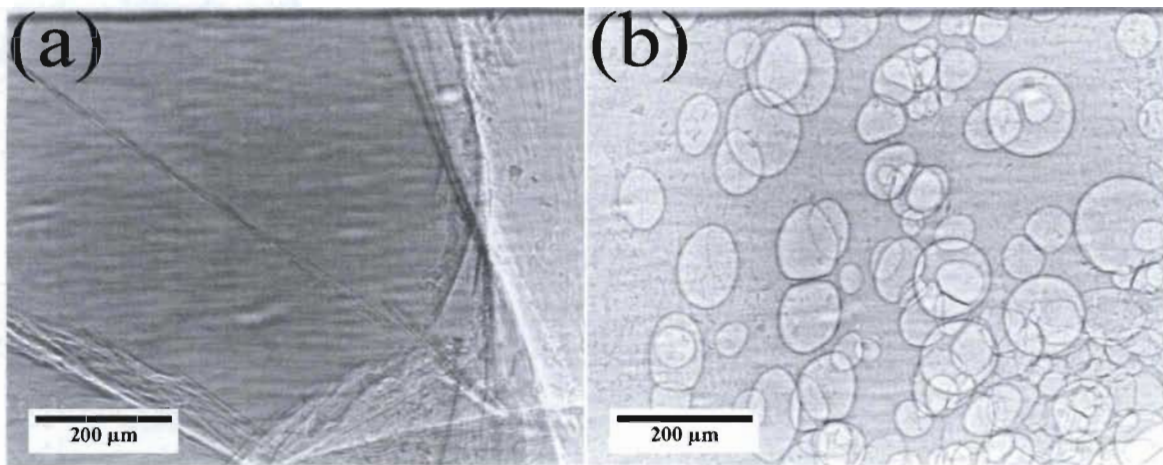


Figure 4. PCI within the bulk of PMMA (a) and Estane (b), showing cracking and voids respectively. The intensity is about 2000 counts.

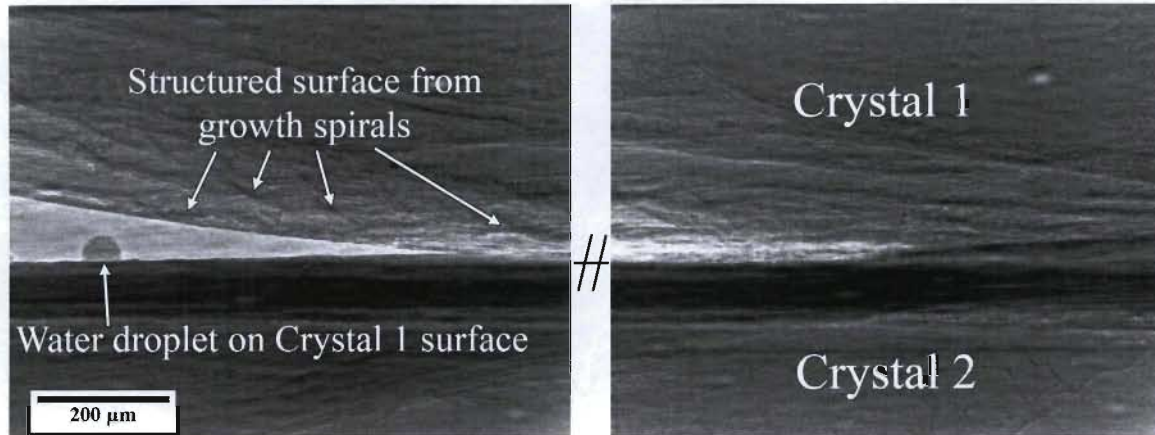


Figure 5. Bicrystal interface resulting from bonding with water. The curvature of the surfaces prevented full bonding, but resolution of the two crystals is apparent. Surface defect structure is observed clearly.

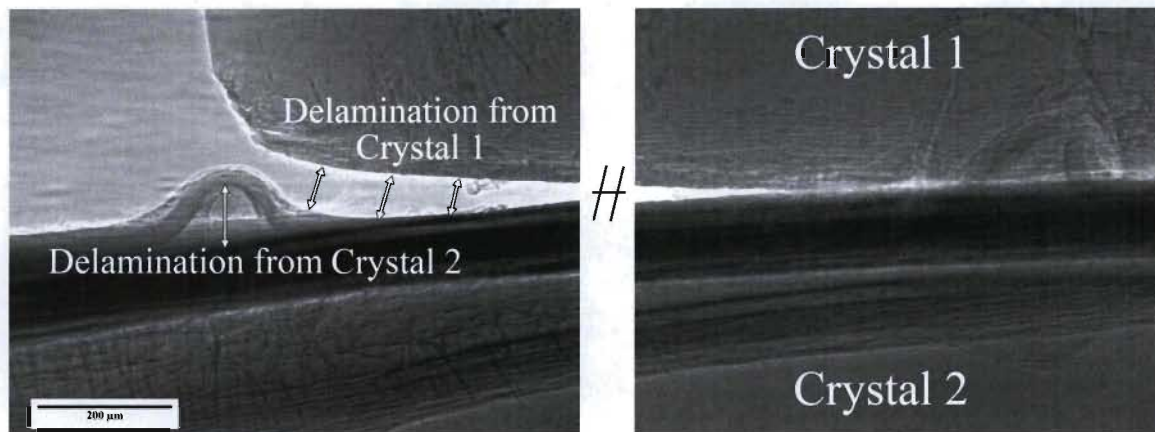


Figure 6. Crystal-epoxy-crystal interface observed by PCI in ENG-2. Crystal 1 appeared to delaminate from the epoxy during the 24 hour cure time, possibly pulling the epoxy with it to create delamination from Crystal 2.

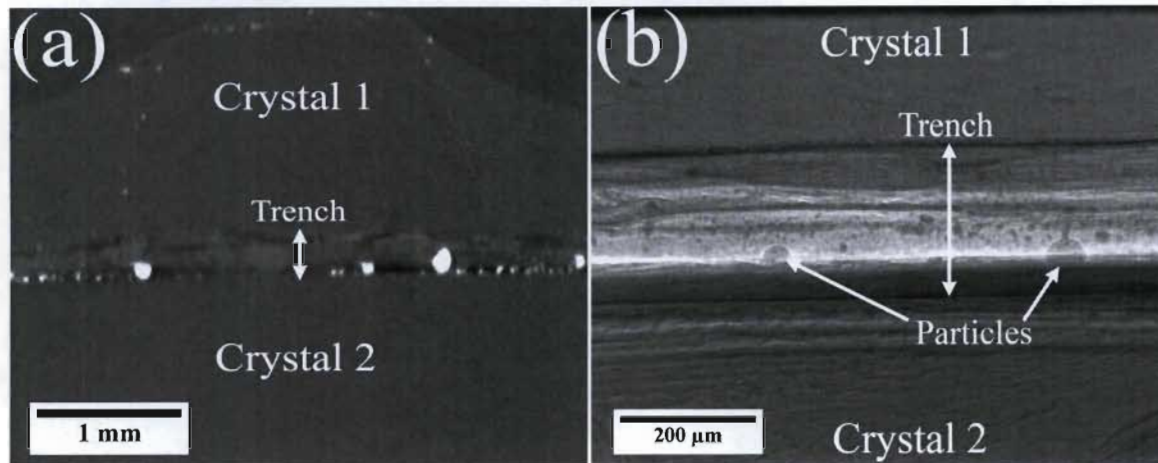


Figure 7. ENG-3 sample characterized with absorption microtomography (a) and synchrotron PCI (b). Doping with  $\text{Bi}_2\text{O}_3$  provided absorption contrast in (a), showing both crystals as well as highlighting the trench effectively. The  $\text{Bi}_2\text{O}_3$  shows up as bright particles in the tomography slice but as dark particles in PCI.

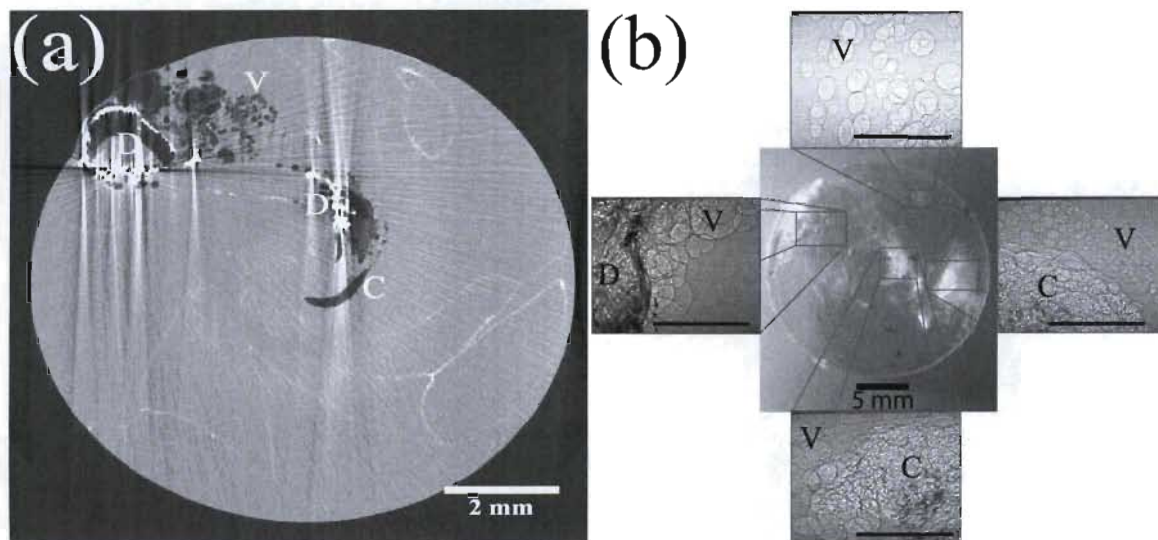


Figure 8. X-ray tomography slice (a) compared with optical microscopy and synchrotron PCI (b) from specified locations in specimen PBS-1. “D” refers to doped crystals or interfaces, “C” refers to non-doped crystals or interfaces, and “V” refers to voids. Scale bars in the PCI images are  $500\ \mu\text{m}$ .

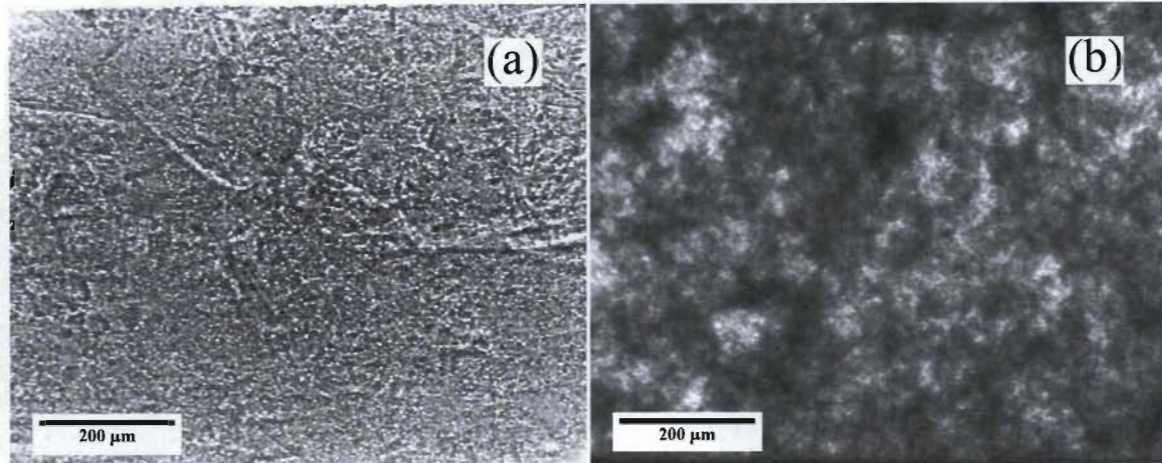


Figure 9. Non-doped (a) and doped (b) PBS samples observed by PCI. Some outlines of crystals are visible but resolution of the microstructure is poor. Both samples were approximately 2 mm thick.

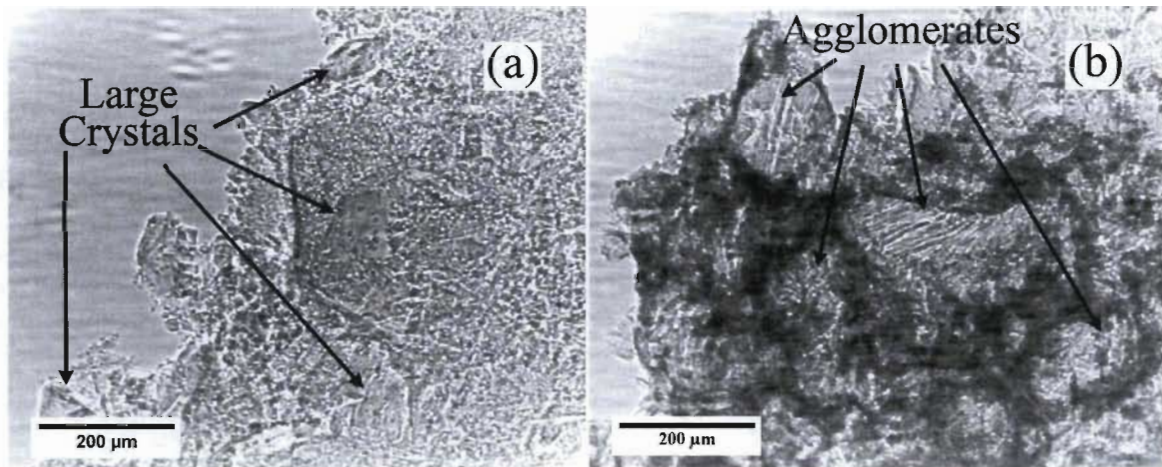


Figure 10. Thin (0.4 mm thick) PBS samples sliced from 2 mm pieces. Several large facets as well as multiple small crystals are visible in the undoped specimen (a), while the doped specimen (b) appears to show crystal-binder agglomerates rather than individual crystals.

## Tables

**Table 1.** List of Formulated Samples for PCI Study

Specimen ID	Description	Bi <sub>2</sub> O <sub>3</sub> Used
CRY-1	Single crystal of sugar	No
CRY-2	Single crystal of acetaminophen	No
PMMA	Cracked PMMA slab	No
ENG-1	Two acetaminophen crystals bonded with water	No
ENG-2	Two acetaminophen crystals bonded with epoxy	Yes
ENG-3	Same as ENG-2 but one crystal had a 250 μm trench	Yes
PBS-1	Acetaminophen pressed into Estane pellet	Yes
PBS-2	Plastic-bonded sugar pellet	No
PBS-3	Plastic-bonded sugar pellet	Yes